Test beam results with LuAG fibers for next-generation calorimeters

PUBLISHED BY IOP PUBLISHING FOR SISSA MEDIALAB

RECEIVED: *August 29, 2013*
ACCEPTED: *September 30, 2013*
PUBLISHED: *October 15, 2013*

Test beam results with LuAG fibers for next-generation calorimeters

M. Lucchini,[a,b,1] **T. Medvedeva,**[c] **K. Pauwels,**[a] **C. Tully,**[c] **A. Heering,**[d] **C. Dujardin,**[e] **K. Lebbou,**[e] **P. Lecoq** [a] **and E. Auffray**[a]

[a] *European Organization for Nuclear Research, CERN, CH-1211 Geneva, Switzerland*
[b] *University of Milano-Bicocca, Piazza dell'Ateneo Nuovo 1, Milano, 20125, Italy*
[c] *Princeton University, Princeton, New-Jersey, 08544, U.S.A.*
[d] *University of Notre Dame, Notre Dame, Indiana, 46556, U.S.A.*
[e] *Institut Lumière Matière, UMR5306 Université Lyon 1-CNRS, Villeurbanne cedex, France*

E-mail: marco.toliman.lucchini@cern.ch

ABSTRACT: For the next generation of calorimeters, designed to improve the energy resolution of hadrons and jet measurements, there is a need for highly granular detectors that require peculiar geometries. Inorganic scintillators can provide good stopping power to allow compact calorimeter designs together with an excellent energy resolution. The micropulling-down technique allows to grow crystal fibers with high aspect ratio providing good granularity. Designs based on dual-readout could also be considered since the host matrices of extrinsic scintillators behave as a Cherenkov radiator in the absence of the scintillating dopant. We report here about results obtained with crystal fibers of 22 cm length and 2 mm diameter of lutetium aluminium garnet (LuAG, $Lu_3Al_5O_{12}$). The response of such fibers in a high energy physics environment has been investigated through a test beam campaign at the CERN PS facility using electrons in the 50–150 GeV energy range. The results, proving the potential of LuAG fibers for calorimetry applications, have been used to validate a Geant4 simulation which allowed to study different configuration of a fiber-based detector. Possible implementations of the crystal fibers technology into a real calorimeter are also discussed.

KEYWORDS: Scintillators and scintillating fibres and light guides; Calorimeters; Scintillators, scintillation and light emission processes (solid, gas and liquid scintillators); Performance of High Energy Physics Detectors

[1] Corresponding author.

doi:10.1088/1748-0221/8/10/P10017

2013 JINST 8 P10017

Contents

2013 JINST 8 P10017

1 Introduction

High Energy Physics experiments at future colliders (e.g. HL-LHC, ILC, CLIC) will have to face challenging operating conditions with unprecedented luminosities and collision rates. The next generation of detectors will require, in addition to excellent timing properties, a significantly better jet resolution, especially in the forward region. To face such requirements, we proposed earlier an approach based on meta-crystals [1, 2]. In this concept, trunks of *cables* constructed from heavy inorganic single crystalline fibers are assembled to form the detector blocks. This solution provides the appropriate segmentation, is dense enough to avoid the necessity of an absorber (thereby excluding sampling fluctuations) and presents dual-readout abilities. With an extrinsic scintillator, both doped and undoped fibers can be assembled to measure respectively the scintillation and Cherenkov signals. The system is then capable of disentangling, on an event by event basis, the electromagnetic (em) and non-em components of a shower with a uniform Moliere radius R_M, radiation and interaction lengths X_0 and λ_I.

The use of Lutetium Aluminium Garnet (LuAG, $Lu_3Al_5O_{12}$) for the assembly of the meta-crystals was proposed earlier [2, 3]. This material combines a high density (6.73 g/cm^3) and relatively short radiation and interaction lengths: X_0 =1.41 cm and λ_I =23.3 cm.

When undoped it is an efficient Cherenkov radiator because of its high refractive index ranging from 2.14 at 190 nm to 1.848 at 520 nm [4, 5] and thus its low Cherenkov threshold (97 keV for electrons). By doping the LuAG matrix with rare-earth ions (e.g. Cerium), fast scintillation processes can also be obtained. Cerium-doped LuAG crystals then yields 25000 photons per deposited MeV [6, 7]. The emitted light is centered at around 520 nm which favors Cherenkov-scintillation separation.

The micropulling-down technology (μPD) makes it possible to grow single crystals of LuAG directly into a fiber shape. As opposed to traditional growth methods (i.e Czochralski or Bridgman techniques), the cutting and polishing of the as-grown ingots can then be avoided with μPD. Furthermore, the rather high pulling rates and the possibility to grow multiples fibers simultaneously give μPD significant advantages for large-scale productions of crystals of high aspect ratio.

Bundles of undoped and Cerium-doped LuAG fibers were already exposed to electron beams during short periods in 2009 and 2010 [8]. For these tests, 20 fibers (diameter of 2 mm and length of 8 cm) of both types were read-out from both ends with photomultiplier tubes and the left-right asymmetry of the recorded signal for different angles of orientation of the fibers with respect to the axis of the incident beam was investigated. Similarly to studies on lead tungstate crystals reported in [9, 10], a strong asymmetry of the undoped LuAG fibers was observed. It was shown that the rather poor quality of the light propagation in these fibers was the key parameter to improve [6]. We reported recently the significant progress achieved which yielded LuAG fibers grown by μPD with attenuation lengths ranging from 30–50 cm depending on the coupling method [11]. A new set of LuAG fibers of higher quality was therefore exposed to an electron beam at the H2 beamline of the CERN SPS north area. As opposed to the previous studies, we decided to readout each fiber separately from both ends using optical fiber and SiPMs (see section 2.2). A selection of 9 fibers, 7 Cerium-doped and 2 undoped, were inserted into a brass absorber, as described in section 2.2. Although this configuration suffers from sampling fluctuations and energy leakage, it allows to investigate the equivalent of a single calorimetric channel. This approach is needed to be able to discuss possible calorimeter designs.

2 Experimental procedures

2.1 LuAG fibers

Single crystalline fibers of LuAG:Ce of 2 mm diameter have been grown at the Institute of Light and Matter (ILM, Lyon, France) by the μPD technique along the $\langle 111 \rangle$ crystallographic axis with an accurate control of the pulling rate and of the applied heating power. The growth process was initiated once a direct contact established between the oriented seed crystal and the capillary die at the bottom of the iridium crucible. The seed was then continuously pulled down at rates ranging from 0.25 to 0.32 mm/min. Technical details of the growth parameters leading to LuAG fibers of higher quality are provided in a separated paper [12]. The main parameters to carefully control are the quality of the raw material and the pulling rate. The obtained LuAG fibers were then cut to a length of 22 cm.

2.2 Mini-CFCAL geometry

A volume of brass was shaped with the tapered geometry (approximately $3\times3\times22\,\mathrm{cm}^3$) of a $PbWO_4$ crystal of the electromagnetic calorimeter endcap (EE) of the CMS experiment. In this

2013 JINST 8 P10017

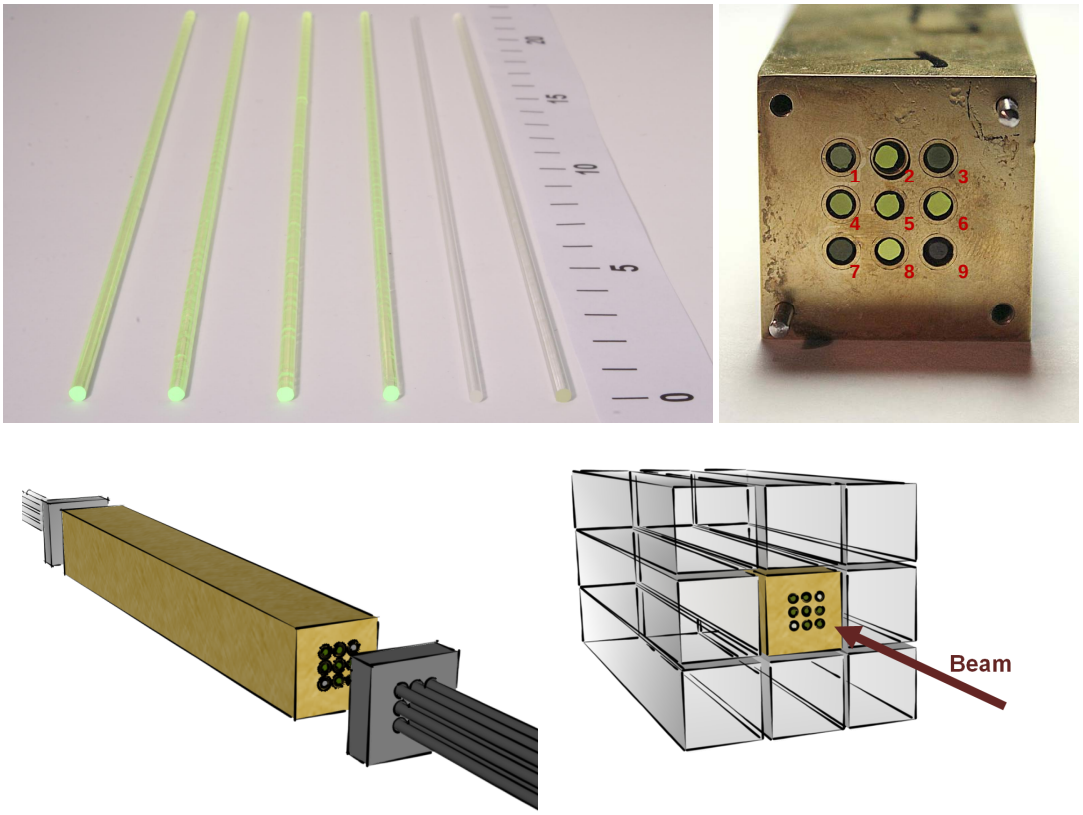

Figure 1. (Top) Pictures of a set of Cerium-doped (green color) and undoped (transparent) LuAG fibers and the brass absorber containing 9 LuAG fibers. (Bottom) The mini-CFCAL (brass absorber with 9 LuAG fibers) is connected to optical fibers for light extraction and inserted in a matrix of $PbWO_4$ crystals.

brass element, 9 LuAG fibers wrapped with Teflon were inserted in holes of 3 mm diameter (see figure 1). As reported in [11], the Teflon wrapping does not enhance the light output or the light propagation, in the case of a long fiber geometry. It was nevertheless decided to use it here to position the LuAG fibers (diameter of 2 mm) in the holes of wider diameter. The Teflon wrapping also protects the fibers when handling the brass element. Two of the nine fibers, the top left (number 1) and the bottom right one (number 9) in the top right picture of figure 1, were undoped LuAG fibers whereas the other seven fibers (number 2,3,4,5,6,7,8) were Cerium doped. In the following, we will refer to this geometry (brass absorber containing 9 LuAG fibers) as mini-CFCAL (miniaturized version of a calorimeter based on crystal fibers).

3 Beam line and test beam setup

The mini-CFCAL has been tested in the H2 test beam line at the Super Proton Synchrotron (SPS) at CERN. A 400 GeV/c primary proton beam extracted from the SPS towards the North Areas splits into three beams one of which is then directed onto the T2 primary target. The proton beam intensity incident on this target is several 10^{12} protons per bunch. The H2 beam is one of the two secondary beams delivered from the T2 primary target by means of the T2 wobbling station which provides flexibility in terms of momentum, charge and intensity of the secondary beams.

2013 JINST 8 P10017

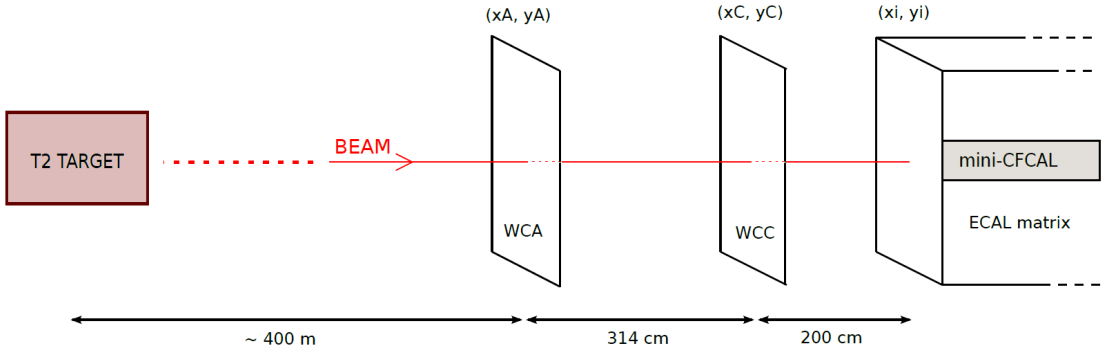

Figure 2. Sketch of the last stage of the H2 beam line at CERN, SPS. The ECAL matrix containing the mini-CFCAL is shown as well as the wire chambers WCA and WCC used in this analysis. The red arrow indicates the electrons beam direction.

The H2 beam line picks up particles emerging from the primary target, makes a selection in terms of momentum and angle and transports them to the user areas.

Several types of detectors allow checks of beam intensities and the beam spot along the beam line and consequently also to correct and optimize the beam steering and focusing. Multiwire proportional chambers (WCA and WCC) shown in figure 2 provide detailed beam profiles and individual particles tracking information. Scintillating counters located upstream from the tested prototype provide the trigger.

For the present study, a beam of electrons with energies of 50, 80, 100, 120 and 150 GeV and intensity around 2000 triggers per spill has been used. The beam size on the target was around $40\times40\,\mathrm{mm}^2$ in order to uniformly cover the whole mini-CFCAL front face.

3.1 Read out electronics and data acquisition system

The mini-CFCAL was inserted in the center of eight neighboring $PbWO_4$ crystals. As shown in figure 1, the electron beam was set parallel to the fibers axis. For the light extraction, each extremity of the mini-CFCAL was coupled with Silicon grease (Rhodorsil Paste 7) to nine cladded plastic fibers which optically transport the analog signal from the fibers ends to the silicon photomultipliers (SiPM).

The SiPMs used are KETEK 20 μm green-sensitive devices with photon detection efficiency (PDE) of $\sim$21% at 520 nm and active area of $2.2\times2.2\,\mathrm{mm}^2$, the gain of which was tunned to be $\sim$1 count per photo-electron by AC-coupling. The charge signal is measured and encoded into a non-linear digital scale by the Charge Integrator IC (QIE) [13]. The QIE uses the LHC clock to divide time into regular bins and measure the accumulated charge in each 25 ns time bin. Internally, the QIE uses capacitors to accumulate the charge and measure the voltage. There are four such capacitors on each QIE, and the QIE uses each capacitor in turn, discharging it for two clocks before using it again. Thus, each subsequent time sample comes from a different capacitor. The outputs of three QIE channels are digitally combined onto a high-speed optical link and sent to the HCAL Trigger/Readout (HTR) board. The HTR board buffers the incoming digital data and transfers it to the Data Concentrator Card which in turn transfers data to the central DAQ [13, 14].

2013 JINST 8 P10017

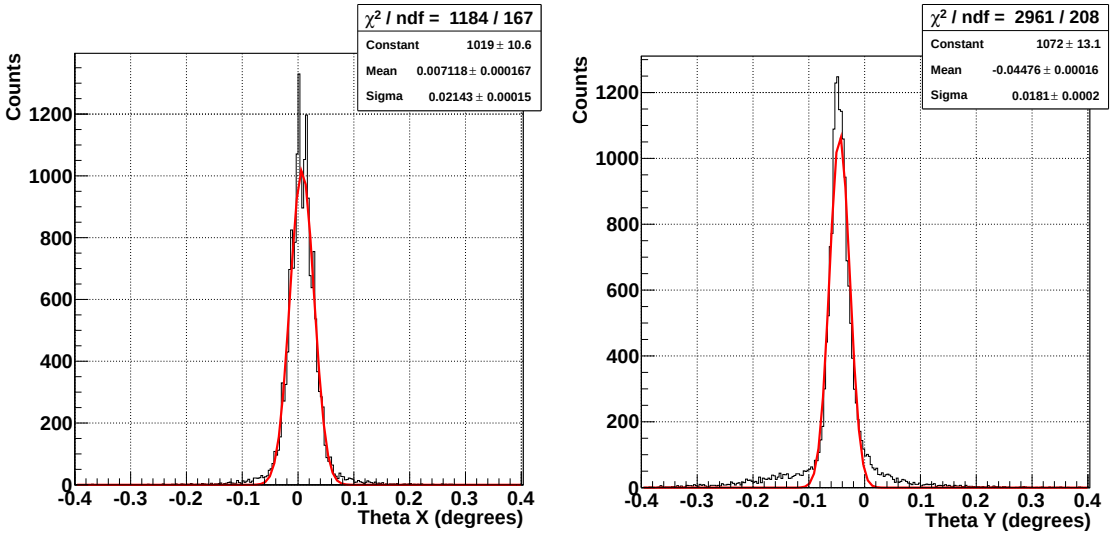

Figure 3. Distribution of particles angle on x (θ_x) and y (θ_y) axis for 80 GeV electrons.

3.2 Wire chambers

Two wire chambers (WCA and WCC) positioned in front of the mini-CFCAL (see figure 2) were used to monitor the impact point of particles on the absorber (x_i, y_i) by extrapolating the particle trajectory:

$$x_i = x_{wca} + (x_{wcc} - x_{wca}) \cdot \frac{z_{wca}}{z_{wca} - z_{wcc}} \tag{3.1}$$

where z_{wca} is the distance of WCA from the absorber, $z_{wca} - z_{wcc}$ is the distance between the two wire chambers and x_{wca}, x_{wcc} are the horizontal coordinates measured by wire chambers WCA and WCC respectively. The information on the particle position allows the study of crystal fibers response as a function of the impact point. The angular spread of the incoming particles was also estimated and results are shown in figure 3. Both on x and y axis the average angle of incoming particles is below 0.1 degrees with small fluctuations, ~ 0.02 degrees, corresponding to $\sim$1 mm spatial resolution at the target location.

4 Test beam results

In this section, the main results obtained in the analysis of the test beam data are described. The response of single fibers is discussed first and the reconstruction of shower profile and shower energy is addressed.

4.1 Response of Ce-doped and undoped LuAG fibers

Two different types of LuAG fibers have been used as active material inside the absorber: Ce-doped fibers to produce scintillation and undoped fibers as Cherenkov radiator. Their response to electrons, with energy between 50 and 150 GeV, has been studied in terms of light output and pulse shape.

2013 JINST 8 P10017

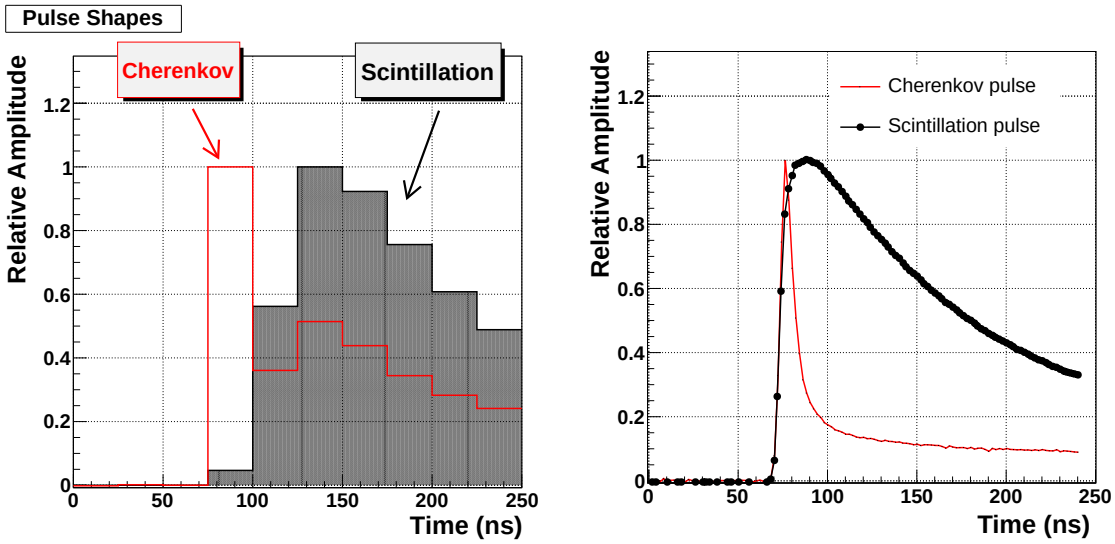

Figure 4. Left: comparison between the average pulse shape of a Ce-doped fiber (black) and an undoped fiber (red) using 80 GeV electrons. Right: average pulse shapes with better time granularity for Ce-doped fibers (black dots) and undoped fibers (red) obtained in previous test beam using an oscilloscope [8].

Using the wire chambers informations a selection of electrons having their impact point within 2 mm radius from the centre of a given fiber was done and the average pulse shape recorded from the two types of fibers was calculated. Results corresponding to 80 GeV electrons are shown in the left plot of figure 4. A clear difference is visible between the Cherenkov pulse (measured with undoped fibers) having a fast decay time < 10 ns and the scintillation pulse (given by Ce-doped fibers) which shows a longer decay time of $\approx$ 60–100 ns. The extra slower component in the undoped fiber was attributed to a Cerium contamination of the Lutetium oxyde. The experimental setup only allowed a 25 ns sampling rate which limits a detailed study of the pulse shape, a more precise measurement of the pulses performed in previous test beams [8] is shown on the right plot of figure 4 for comparison.

Applying the same beamspot selection, the distributions of signal induced by 80 GeV electrons in the two types of fibers were obtained. The signal of each SiPM has been converted in number of photolectrons using conversion factors C^i obtained by calibrating each SiPM channel with LEDs signals. Ce-doped fibers, as expected, show a much higher signal ($\sim$ 1800 photoelectrons) with respect to the undoped fibers ($\sim$ 80 photoelectrons), see figure 5. These values correspond to photoelectrons measured from the back end of a given fiber, hence this number will increase for scintillating fibers, by a factor ~ 2, if also the front end signal of each fiber is considered. Furthermore, a fraction of the photons is absorbed inside the optical fibers used to transport the signal from the crystal fiber end to the SiPMs.

4.2 Transverse granularity

To investigate the response of fibers as a function of the electrons impact point we made use of the wire chambers information to scan along x and y axis the whole mini-CFCAL. After a selection of events within ± 5 mm on the y axis, the average response of a given fiber while changing the

2013 JINST 8 P10017

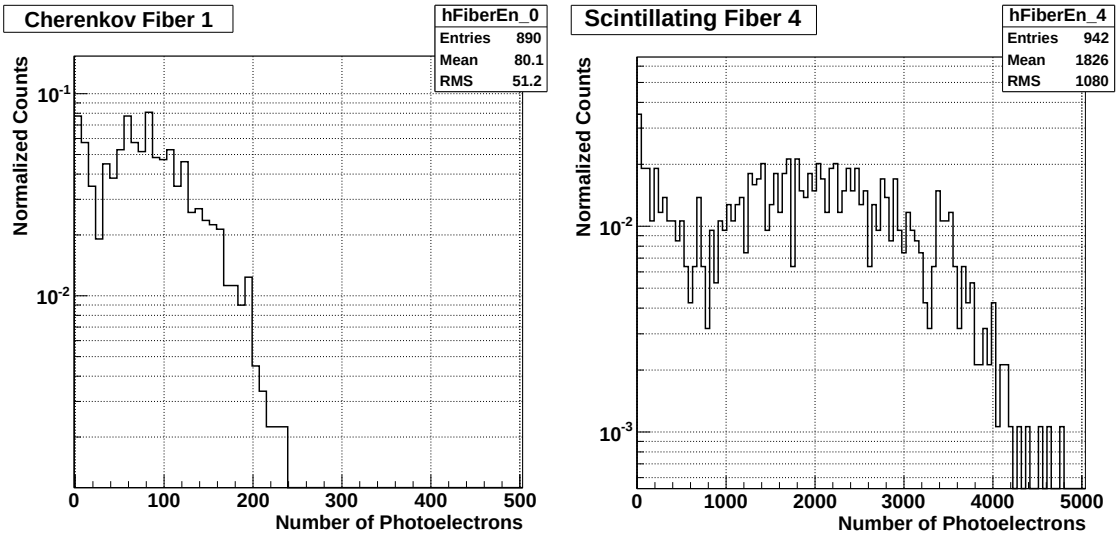

Figure 5. Distribution of photoelectrons measured from one end of a Cherenkov fiber (left) and a scintillating fiber (right) using 80 GeV electrons within a $2\times2\,\mathrm{mm}^2$ beamspot around the centre of the selected fiber.

impact point on the x axis was calculated. The same procedure was performed for the y axis. The maximum values IC_x and IC_y of these transverse profiles correspond to the average response of the fiber when the impact point is equivalent to the fiber position, on the x and y axis respectively. These coefficients are proportional to the light output of each fiber. Therefore, we can then define intercalibration coefficients between fibers as:

$$IC^i = \frac{IC^i_x + IC^i_y}{2} \tag{4.1}$$

This intercalibration procedure is necessary to normalize the signal from different fibers in order to take into account for their different light output which is related to the Cerium concentration, the fiber quality and the optical coupling between crystal fibers, optical fibers and SiPMs. The normalized distributions for the central row and central line fibers are shown in figure 6. Transverse profiles on the y axis show narrower peaks around the fiber positions reflecting the higher quality of the beam profile on the y axis with respect to the x axis.

4.3 Energy reconstruction

Applying intercalibration coefficients, the particle energy can be reconstructed using the contribution from different fibers in order to collect the maximum fraction of energy deposited by the shower in the mini-CFCAL. Events within a beamspot of 5 mm radius around the central fiber have been selected in order to consider only electrons which starts the shower inside the array of fibers. The contribution of each fiber, after intercalibration, has been summed up event by event to reconstruct the signal:

$$E_{\mathrm{reco}} = \sum_{i=1}^{9} S^i_{\mathrm{front}} \cdot C^i \cdot IC^i \tag{4.2}$$

2013 JINST 8 P10017

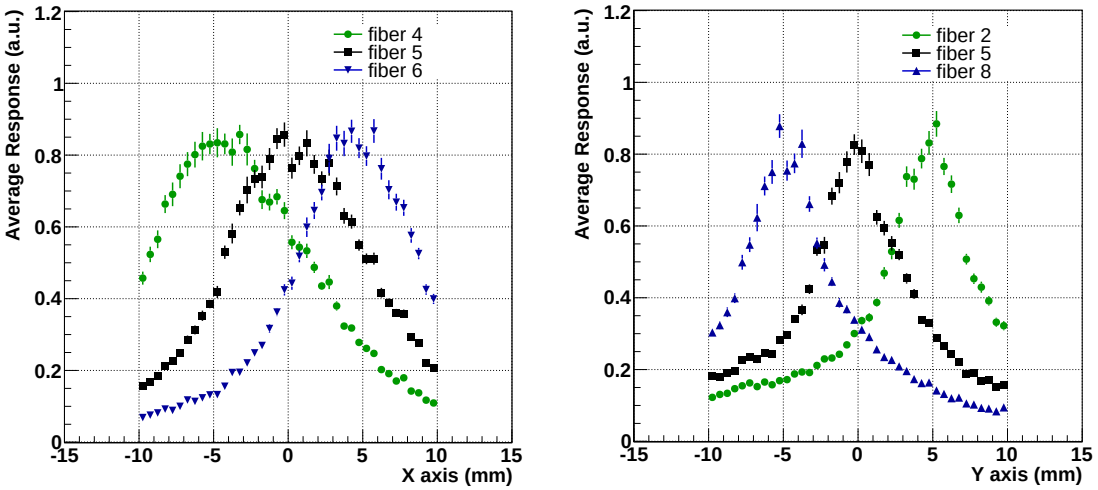

Figure 6. Left: average response of the fibers of the central row as a function impact point along the x axis: fiber 4 (green), fiber 5 (black), fiber 6 (blue). Right: average response of the fibers of the central line as a function impact point along the y axis: fiber 2 (blue), fiber 5 (black), fiber 8 (green).

where S^i_{front} is the signal measured from the front end of each fiber i, C^i are calibration factors to convert the SiPM channel into photoelectrons, obtained using a LED signal as reference, and IC^i are the intercalibration coefficients.

For the energy reconstruction only signals from the front end of the fibers have been used, since for two fibers (namely fiber 3 and fiber 5) the back signal was not available because of a wrong tuning of the corresponding SiPM voltages. If all back readouts were available, reconstructing the signal using both front and back signals could slightly increase the resolution because of the higher photostatistics. Using electrons at different energies between 50 and 150 GeV, we studied the evolution of the fibers array response. Obtained distributions of the reconstructed amplitude E_{reco} are then fitted with a Gaussian function to estimate the peak position which shows a good correlation with the beam energy as shown in the right plot of figure 7. The energy resolution of the reconstructed amplitude varies from 15% to 20% and it is dominated by a constant term due to the transverse non uniformity of the response and several experimental systematics discussed in section 5.

4.4 Longitudinal shower profile

While increasing the energy E of incoming electrons, the position of the shower maximum t_{max} moves towards the back of the absorber according to:

$$t_{\text{max}} \propto \ln(E) \tag{4.3}$$

This change in the shower profile along the longitudinal axis (z) is expected to produce a different ratio of the front and back signals measured at the two opposite ends of each fiber. We can define a dimensionless estimator of the shower maximum position as follows:

$$R_{BF} = \ln\left(\frac{S_{\text{back}}}{S_{\text{front}}}\right) \tag{4.4}$$

2013 JINST 8 P10017

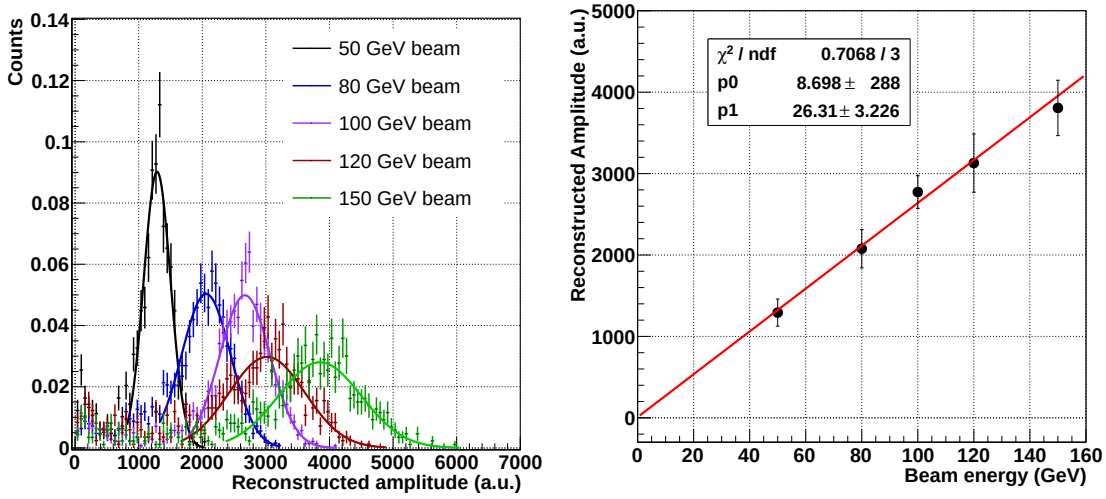

Figure 7. Left: distributions of reconstructed amplitude E_{reco} at different beam energy. Right: correlation between the peak value of E_{reco} distributions and the beam energy with a linear fit (red line). Error bars represent the statistical error on the estimation of peak position.

where S_{front} and S_{back} are respectively the signals measured at the front and back end of a fiber. The value of R_{BF} has been estimated for both Cherenkov and scintillating fibers using different beam energy in the range from 50 to 150 GeV. A beamspot selection of 5 mm around the selected fiber has been applied in order to reduce the noise background. In figure 8, results obtained with the Cherenkov fiber number 1 are shown. We observed a clear correlation between the value of R_{BF} and the beam energy which demonstrates the feasibility of longitudinal shower profile studies using a double readout technique. Similar results are obtained using the scintillating fiber number 4 and are shown in figure 9.

The different nature of scintillation and Cherenkov light, the former being emitted isotropically whereas the latter has a favorite direction, can explain the difference between the two type of correlations. As expected, the Cherenkov fiber shows a much higher signal in the back readout with respect to the front one.

The value of R_{BF} is also expected to show a correlation with the impact point of electrons (along the x and the y axis) since the fraction of the electromagnetic shower which interacts with a fiber will move towards the back end when the shower develops far from the fiber position, as represented in the naive sketch of figure 10. To study the effect of the impact point on the value of R_{BF}, we selected events within concentric rings at a given distance from the selected fiber and calculated the average value of R_{BF} for each ring. Results are shown in the right plot of figure 10. As expected, we observe a significant correlation between the distance of the electron impact point from a fiber and the value of R_{BF}. The back signal proportionally increases with respect to the front signal when electrons are generating the shower further from the fiber. In such conditions, only a small fraction of the shower interacts with the fiber reducing the scintillation signal which, in turn, increases the sampling fluctuations.

2013 JINST 8 P10017

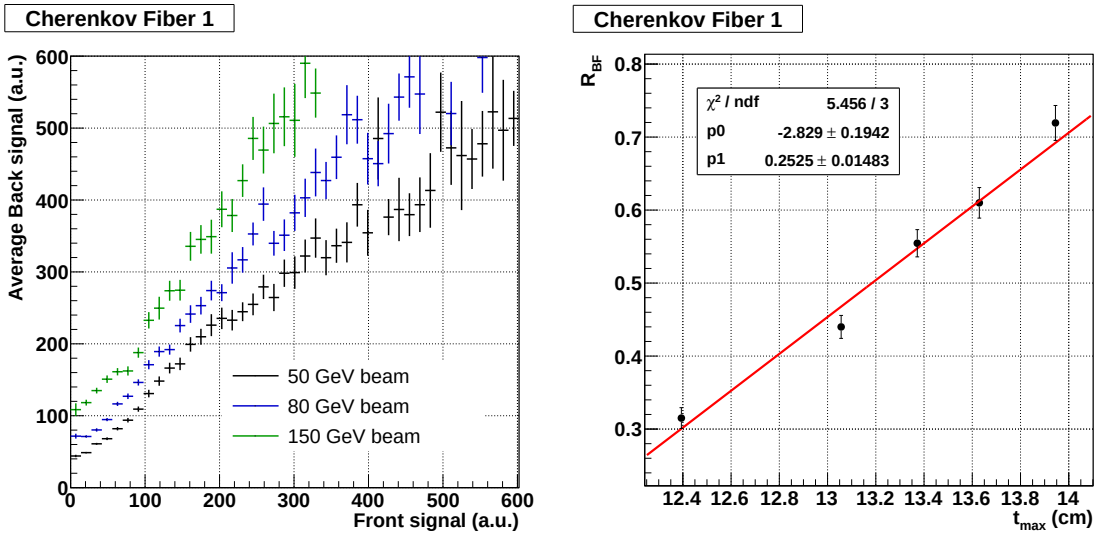

Figure 8. Left: the correlation between front F and back B signals of Cherenkov fiber number 1 is shown at different beam energy. Right: correlation between R_{BF} and the theoretical $t_{\max}$ position for a given beam energy with a linear fit (red). Error bars represent the statistical uncertainty on the points.

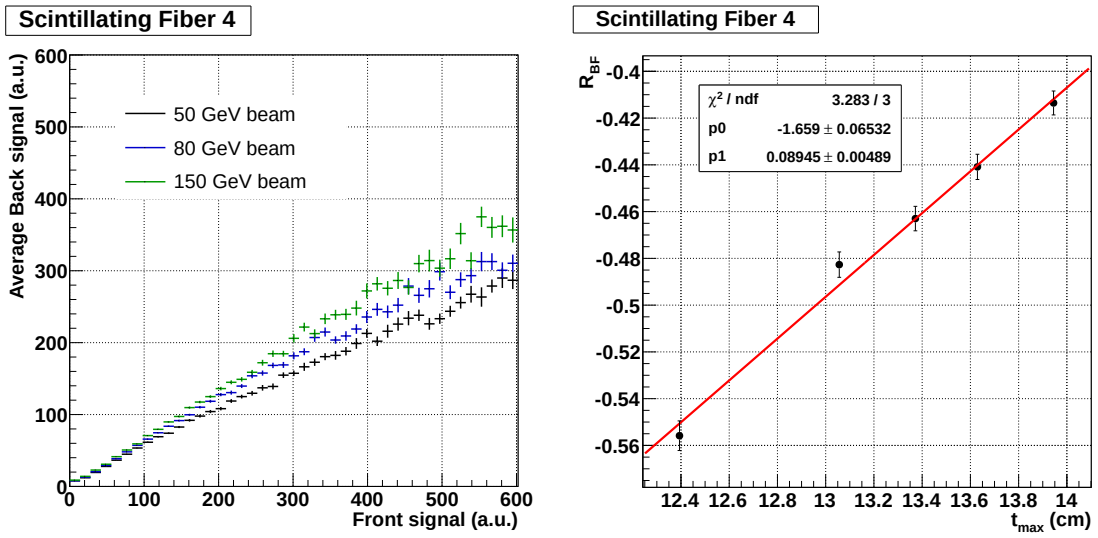

Figure 9. Left: the correlation between front F and back B signals of scintillating fiber number 4 is shown at different beam energy. Right: correlation between R_{BF} and the theoretical $t_{\max}$ position for a given beam energy with a linear fit (red). Error bars represent the statistical uncertainty on the points.

5 Discussion

The test beam results presented in this paper confirm the potential of LuAG fibers for high energy physics applications. A significant amount of light was extracted from both the Cherenkov and the scintillating fibers. The response of single fibers to electrons depends on the impact point of the particle and thus it can be used to study the transversal profile of the shower. Combination of the signals from clusters of adjacent fibers can be used to build algorithms which allow an estimation of the particles impact point and angle.

2013 JINST 8 P10017

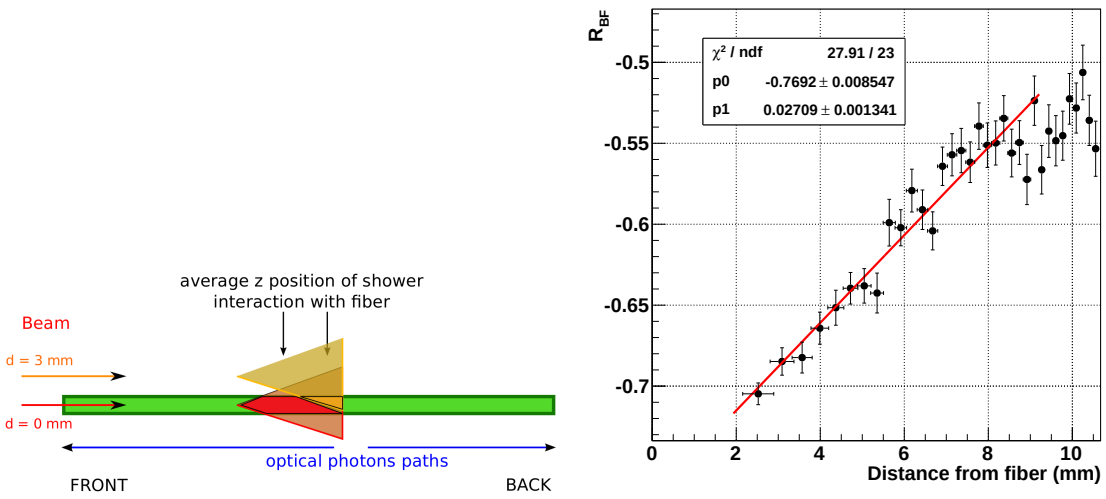

Figure 10. Left: a sketch to naively represent the drift of the average interaction point of the shower with a given a fiber when the electron impact point move away from the fiber centre. Right: correlation between the value of R_{BF} and the position the distance of electrons from the fiber. A linear fit is performed in the range (2,9) mm distance (red line). Error bars represent the statistical uncertainty on the points.

The feasibility of using double readout (i.e. make use of signal from both front and rear ends of each fiber) to increase the knowledge on the shower profile along the fiber axis has been investigated. Good correlations of the back and front signals ratio R_{BF} with the shower maximum position (along z axis) and with the impact point of electron on the mini-CFCAL front face (x, y axis) were found. The optimization of the double readout can provide even more informations on the longitudinal shower profile without the necessity to increase the longitudinal segmentation and hence the number of channels.

More issues related to the real potential of such calorimeter in the context of particle flow algorithms or dual readout corrections (i.e. reading out the scintillation and Cherenkov light separately on a event by event basis to correct for hadronic shower fluctuations) are not addressed in this paper because of the small dimensions for this prototype and to the low number of fibers involved. Nevertheless, current data can be used to validate simulation tools in order to investigate new geometries and configurations. A Geant4 simulation [15] has been performed to allow a first comparison with data and to investigate the potential of a larger array of fibers in terms of energy resolution.

The same geometry of the mini-CFCAL, in terms of fiber packing, has been simulated extending the array of fibers to a 41×41 matrix inserted in a brass absorber with transverse dimensions of $22\times22\,\mathrm{cm}^2$. Such geometry, shown in figure 1, will be referred as Geometry A. A different geometry (Geometry B) was also simulated, in which the gap between the fibers and the absorber (resulting from the 0.5 mm layer of Teflon) has been reduced to 0.1 mm. An hexagonal packing was chosen here so that the spacing between fibers centres is reduced to 3 mm (see figure 11). In this case, a 123×123 matrix of 22 cm long fibers is needed to fill a brass block of $\sim 33\times33\times22\,\mathrm{cm}^3$.

Electrons of energy between 1 and 150 GeV, uniformly spread on a $10\times10\,\mathrm{mm}^2$ area and with a small angular spread of 5 mrad, which aims to reproduce the experimental conditions of the test

2013 JINST 8 P10017

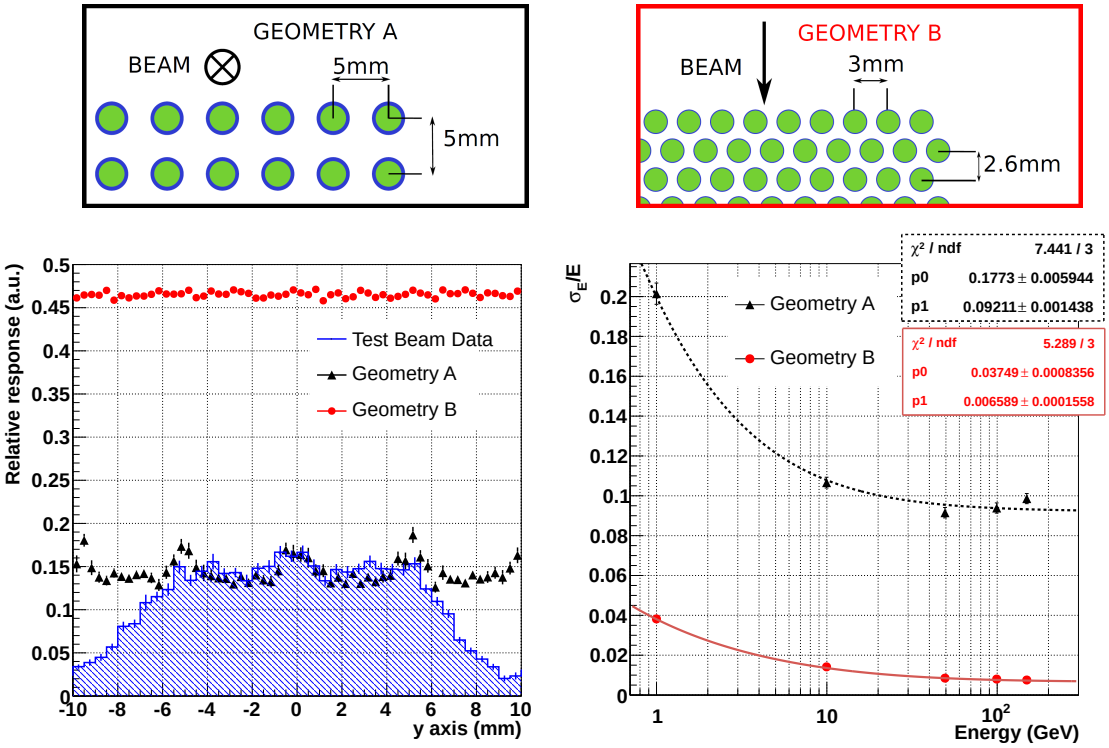

Figure 11. Top: a sketch of Geometry A (left) and Geometry B (right). The blue gaps between fibers (green) and the absorber (white) represent the Teflon layers. The beam direction is also illustrated for the two configurations. Bottom left: fraction of electron energy deposited in the array of fibers as a function of a 50 GeV electron impact point along y axis for Geometry A (black) and Geometry B (red). Experimental data points are shown with a blue line. Bottom right: energy resolution curves for Geometry A (black) and Geometry B (red) at different beam energies fitted using $\sigma_E/E = \sqrt{p_0^2/E + p_1^2}$ where p_0 and p_1 represent the stochastic and the constant term respectively.

beam, have been simulated. For Geometry A, the electrons direction was oriented in the same configuration as in the test beam whereas for Geometry B the electrons beam direction was set perpendicular with respect to the fiber axis in order to reduce the non-uniformity of the response. The energy deposited by the electromagnetic shower inside the active volume of LuAG fibers has been measured and allowed to study the transversal non-uniformity of the response as shown in figure 11. We can observe that the response of the mini-CFCAL decreases when the impact point of electrons is out of the fiber array of ± 5 mm. In both data and simulation of Geometry A the response fluctuates periodically when the impact point moves from the center of the fibers to the brass between adjacent fibers. When the granularity and the packing configuration are improved (for instance in Geometry B), the total fraction of the shower collected in the active volume is increased by a factor $\sim$3 and the non-uniformity of the response is reduced.

The evolution of energy resolution with respect to the electron energies is shown in the right plot of figure 11. Of particular interest, is the resolution that can be achieved with the granularity of Geometry B in a non-pointing fibers configuration which has a stochastic term of $\sim$ 3.7% and a constant term of $\sim$0.7% due to partial containment of the shower and sampling fluctuations.

2013 JINST 8 P10017

Such a good resolution is achieved by means of tilting the detector of 90° which results in a better transverse uniformity of the response which was one of the main limitation to the energy resolution of Geometry A.

The predicted energy resolution for Geometry A (∼10%) is better than the experimental resolution of the distributions in figure 7 which is ∼15–20%. The difference is related to several factors: a poorer transverse containment of the shower due to the smaller array of fibers in the mini-CFCAL, the contribution of the electronic noise, the limited precision of intercalibration coefficients between fibers and other systematics related to the experimental setup and beam quality.

6 Perspectives and outlook

Supported by the results obtained with this first test beam campaign, it is worth to investigate possible designs to implement this technology in a real calorimeter for high energy physics. Although, in the present study, only the response to electrons has been deeply investigated, the potential of a crystal fiber calorimeter to improve the resolution of hadronic showers using dual readout techniques was previously investigated in [8]. It was demonstrated that a fraction of active volume similar to the one of Geometry B (around 45%) would allow to apply dual readout corrections which can improve the energy resolution of hadronic shower reducing the stochastic term below 30%. Also different configurations with different fraction of sensitive volume and Cherenkov/scintillation component were studied [8].

In addition to the dual readout potential of this material, the good energy resolution to electromagnetic shower that can be achieved with configurations similar to Geometry B (top right sketch in figure 11) suggests the feasibility to integrate an electromagnetic and a hadronic calorimeter into a new type of detector which can satisfy both requirements.

In particular, the very peculiar shape of crystal fibers, which can be grown with different diameters and lengths, turns out to be a very flexible tool which allows to optimize their implementation into a calorimeter. A possible way of packing crystal fibers, in order to fill a big and shaped volume like the one of a real detector, is shown in figure 12. Several fibers of variable length between 1.5 and 7 cm are grouped together into a “ladder”-like structure in which the signals from all the fibers are readout by means of a light guide (i.e. a wavelength shifter and quartz capillary system) which transports the signal to the photodetector. Within a “fiber-ladder”, the composition of scintillating and Cherenkov fibers as well as the spacing between them can be varied to optimize the detector perfomance and reduce the cost. The Cherenkov and the scintillating signals could be readout using two separate light guides which collect the light from the two opposite ends of the fibers. This particular “ladder”-like structure allows to minimize the optical path of photons inside the active volume of crystal fibers reducing the time jitter and the light absorption.

These “fiber-ladders” can then be assembled into wedges of different size and shape in order to fit a projective geometry. The length of the “ladders” and the spacing between them can be used to tune the fiber granularity along the longitudinal and radial coordinates in order to better fit the detector requirements.

2013 JINST 8 P10017

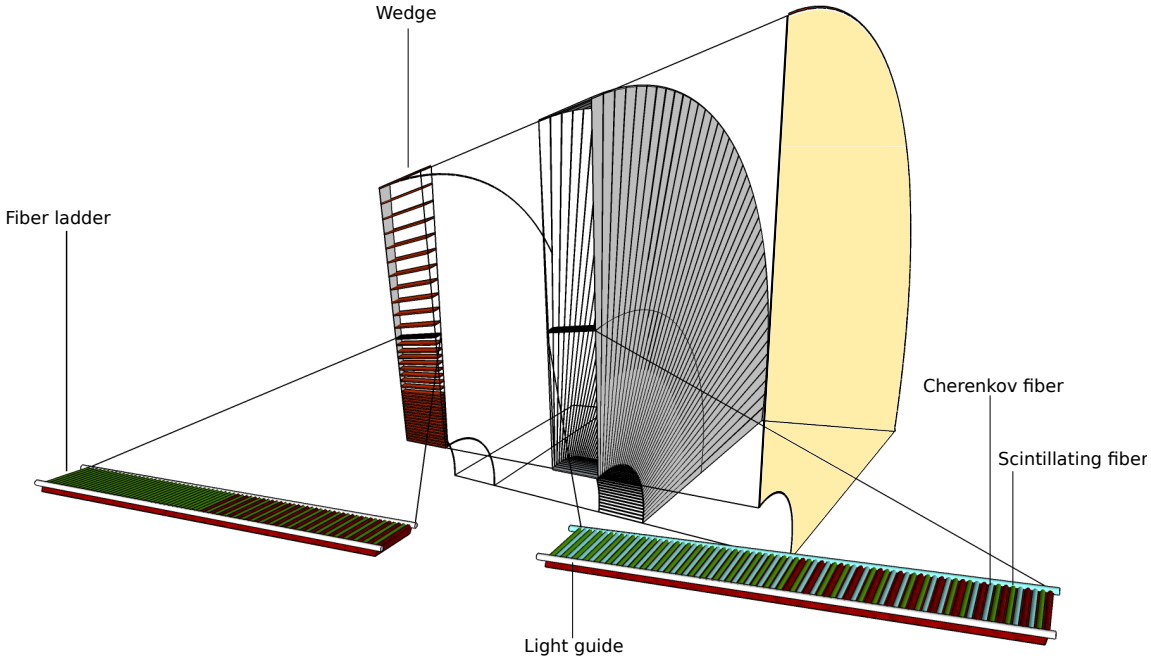

Figure 12. Possible implementation of crystal fibers into a real calorimeter of $\sim$ 1.7 m length and external radius varying from 1.2 to 2.4 m shaped into a projective geometry with respect to the interaction point. The basic cell consists of a $3\times22\,\mathrm{cm}^2$ "ladder"-like structure made of brass (or another absorber) which contains several Cherenkov (blue) and scintillating (green) fibers of 2 mm diameter readout by two separate light guides (white) which transport the signal to the photodetectors. These basic cells are then assembled into shaped wedges to fill the whole detector volume. Two separate layers are shown, the one closest to the interaction point might correspond to an electromagnetic calorimeter with high granularity and the second layer could represent a first part of a hadronic calorimeter with lower granularity and dual readout option implemented (i.e. reading out the scintillation and Cherenkov light separately).

7 Conclusions

The test beam study presented in this paper, demonstrates the potential of LuAG crystal fibers for high energy physics calorimeters. The fibers tested here, which can be used either as scintillator or as Cherenkov radiator, led to a good signal extraction.

The small prototype (mini-CFCAL), which was tested at CERN SPS facility with electrons of energies between 50 and 150 GeV, can be considered equivalent to a single calorimetric channel. It allowed to reconstruct the energy of electrons with good energy linearity and to study the shower profile transversally and longitudinally by means of the fiber granularity and of the double readout (front and rear ends of each fiber).

Present results have been used to validate a Geant4 simulation tool which allow to investigate the potential of a larger array of fibers in the context of electromagnetic and hadronic calorimeters for high energy physics. By tuning the fraction of active volume and the configuration of fibers inside the detector a good energy resolution to electromagnetic particles can be achieved.

Further test beam studies are planned to deeply investigate different fibers configuration into a larger prototype and its response to hadronic shower especially in terms of tracking, shower profile reconstruction and dual readout.

2013 JINST 8 P10017

Acknowledgments

Research is conducted in the frame of the Crystal Clear Collaboration. We acknowledge support from the French National Agency for Research under grand agreement ANR-10-BLAN-0947 (INFINHI). The test beam study has been done within the framework of the CMS collaboration and we would like to thank our CMS collegues who made available the test beam facility. The funding support for the Princeton University group comes from DOE Award # ER-41850.

References

[1] P. Lecoq, *Metamaterials for novel X- or γ-ray detector designs*, *IEEE Nucl. Sci. Conf. R.* (2008) 1405.

[2] P. Lecoq, *New crystal technologies for novel calorimeter concepts*, *J. Phys. Conf. Ser.* **160** (2009) 12016.

[3] E. Auffray, D. Abler, P. Lecoq, C. Dujardin, J. Fourmigue and D. Perrodin, *Dual readout calorimeter with heavy scintillating crystal fibers*, *IEEE Nucl. Sci. Conf. R. (NSS/MIC)* (2008) 3262.

[4] M. Letz, A. Gottwald, M. Richter, V. Liberman and L. Parthier, *Temperature-dependent Urbach tail measurements of Lutetium Aluminum garnet single crystals*, *Phys. Rev.* **B 81** (2010) 155109.

[5] Y. Kuwano, K. Suda, N. Ishizawa and T. Yamada, *Crystal growth and properties of* $(Lu,Y)_3Al_5O_{12}$, *J. Cryst. Growth* **260** (2004) 159.

[6] C. Dujardin et al., *LuAG:Ce fibers for high energy calorimetry*, *J. Appl. Phys.* **108** (2010) 13510.

[7] J.A. Mares et al., *Scintillation properties of* Ce^{3+} *- and* Pr^{3+} *-doped LuAG, YAG and mixed* $Lu_xY_{1-x}AG$ *Garnet Crystals*, *IEEE T. Nucl. Sci.* **59** (2012) 2120.

[8] G. Mavromanolakis, E. Auffray and P. Lecoq, *Studies on sampling and homogeneous dual readout calorimetry with meta-crystals*, 2011 *JINST* **6** P10012.

[9] N. Akchurin et al., *Dual-readout calorimetry with lead tungstate crystals*, *Nucl. Instrum. Meth.* **A 584** (2008) 273.

[10] E. Auffray, D. Abler, P. Lecoq and G. Mavromanolakis, *Dual readout with PWO crystals and LuAG crystal scintillating fibers*, *IEEE T. Nucl. Sci.* **57** (2010) 1454.

[11] K. Pauwels et al., *Single crystalline LuAG fibers for homogeneous dual-readout calorimeters*, 2013 *JINST* **8** P09019.

[12] X. Xu et al., *Growth parameters optimization for LuAG:Ce scintillating fibers pulled by the micro-pulling down technique*, *J. Cryst. Growth* (2013) to be published.

[13] CMS collaboration, *CMS Technical Design Report for the Phase 1 Upgrade of the Hadron Calorimeter*, CERN-LHCC-2012-015, CMS-TDR-010, pg. 51–66.

[14] E. Hazen, J. Rohlf, S. Wu, A. Baden and T. Grassi, *The CMS HCAL data concentrator: A modular, standards-based implementation*, in proceedings of *7th Workshop on Electronics for LHC Experiments*, pp. 347–350.

[15] GEANT4 collaboration, S. Agostinelli et al., *GEANT4: A Simulation toolkit*, *Nucl. Instrum. Meth.* **A 506** (2003) 250.

2013 JINST 8 P10017